Research Article
doi.org/10.1002/cssc.202200456
Chemistry Europe
European Chemical Societies Publishing

Investigating Molecular Transformation Processes of Biodiesel Components During Long-Term Storage Via High-Resolution Mass Spectrometry

David Hamacher[a] and Wolfgang Schrader*[a]

Biodiesel is an important building block in renewable energy transformation. The main issue is that during storage biodiesel will undergo transformation processes that can lead to molecular changes, which then can cause applicational problems such as severe motor damage. To prevent this, a detailed understanding of the involved molecules and the emerging aging products is necessary. Biodiesel samples were stored for up to 12 months to monitor molecular changes, and all mixtures were investigated by using ultrahigh-resolution mass spectrometry (HRMS) with electrospray ionization (ESI). The data revealed that during storage large numbers of oxygen atoms were incorporated into the fatty acid methyl esters (FAMEs). This process was dominant for the first quarter of aging but then became overshadowed by dimerization of oxygenated FAMEs. This means that there are two main pathways for aging in biodiesel: polyoxygenation and oligomerization. These findings greatly pin down the possible causes for sedimentation giving a solid foundation for aging inhibition development.

Introduction

It is undeniable that fossil fuels are a finite resource.[1] Hence, and because of the fatal influence on global warming by burning such fuels,[2] the way of transportation and storage, production and distribution of energy needs to change in the near future towards cleaner and renewable sources. Among others, the utilization of biodiesel is one possibility to achieve a smooth transition. It allows the reduction of fossil fuel usage, the emission of toxic exhaust gases, and to lessen the negative impact on the environment, while keeping the established infrastructure still intact. Biodiesel is widely used in commercial diesel fuel and blended with fossil diesel.[3] Biodiesel mainly consists of fatty acid methyl esters (FAMEs), which are gained by transesterification of biologically produced oils.[4] These oils can come from a great variety of sources, such as rapeseed or palm oil. In Germany, rapeseeds or used cooking oils are the dominant sources.[5] More recent approaches use algae[6] or even yeast grown on orange peel waste to produce FAMEs.[7] Based on the origin, biodiesel is categorized into different generations.[8] Biodiesel produced from rape seed (RME) is considered a first-generation biodiesel because it is produced from an edible plant source, whereas biodiesel made out of used cooking oils (UCOME) is typically considered a second-generation fuel because it is a waste product, and thus derived from a non-edible source. The source material used for their production also influences the individual ratio of the FAMEs present in a biodiesel.[9] The most common FAMEs in biodiesel are derived from their corresponding C16:0 and C18:0–3 fatty acids (see insets in Figure 1). The first number represents the number of carbon atoms in the fatty acid chain and the latter number indicates the amount of double bonds present in the alkyl chain. This degree of unsaturation is directly related to a FAME's susceptibility to autoxidation, C18:3 being 97 times and C18:2 40 times more reactive than C18:1.[10]

Although using biodiesel over fossil fuels has certain advantages, such as reducing the CO_2 output, less particulate matter emission,[11] and higher lubricity,[12] it is also accompanied with a few downsides. Of primary concern is the susceptibility of biofuels to oxidation. They have shown sensitivity towards oxidation in general, which has been studies using stability tests, like PetroOxy and Rancimat.[13] These formed biodiesel oxidation products can corrode metal[14] and form precipitates, which may clog filters and pumping systems.[15] The products of such reactions and the reaction pathways leading to them have been the scope of many

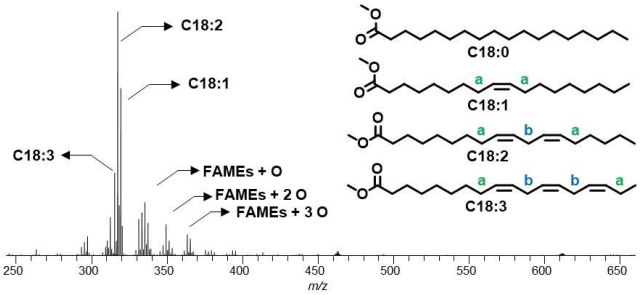

Figure 1. Mass spectrum of UCOME before storage, and the structures of the measured FAMEs with marked allylic (a) and bis-allylic (b) positions.

[a] D. Hamacher, Prof. Dr. W. Schrader
Max-Planck-Institut für Kohlenforschung
Kaiser-Wilhelm-Platz 1, 45470 Mülheim an der Ruhr (Germany)
E-mail: wschrader@kofo.mpg.de

Supporting information for this article is available on the WWW under https://doi.org/10.1002/cssc.202200456

© 2022 The Authors. ChemSusChem published by Wiley-VCH GmbH. This is an open access article under the terms of the Creative Commons Attribution Non-Commercial NoDerivs License, which permits use and distribution in any medium, provided the original work is properly cited, the use is non-commercial and no modifications or adaptations are made.

© 2022 The Authors. ChemSusChem published by Wiley-VCH GmbH

studies. Frankel laid the groundwork to many of those.[10] He described the hydrogen abstraction from the allylic and especially the bis-allylic positions in fatty acids (see insets in Figure 1) and the resulting formation of hydroperoxides on the terminal positions of the so-formed pentadienyls. These hydroperoxides can then react in numerous ways, for example, under epoxide formation or β-scission to build smaller hydrocarbons, aldehydes, or enols. Based on this, Flitsch et al. monitored the formation of short fatty acids (C_5–C_9) during accelerated aging of biodiesel and epoxides of methyl oleate using gas chromatography with a flame ionization detector (GC-FID).[16] Studies observing the deterioration of fatty acids due to high thermal stress during frying processes report the findings of hydroxides, ketones, and epoxides of various chain length after thermooxidation.[17] Another proposed consequence of the hydroperoxide formation is dimerization of the fatty acids by building peroxide cross-links between two oxidized esters.[18] Many studies using analytical setups build around GC for the investigation of fatty acid aging. While reliable and well-studied, the usage of GC limits the investigation in terms of concentration and polarity of the analytes. Another limitation is that in GC all analytes are being heated, which can cause reactions and alterations in the original analytes. GC-FID is an excellent method to measure concentrations of unaltered esters, but it only provides very sparse information about the structural composition of aging products. While gas chromatography-mass spectrometry (GC-MS) can provide these, the method still has the same thermal limitations mentioned before and often utilizes electron ionization (EI), a hard ionization method, which more often than not will fail to provide molecular ion signals. Direct-injection electrospray mass spectrometry (ESI-MS) is a soft ionization technique, which could provide these molecular ion peaks, and no excessive heat exposure of the analytes is necessary. Although there are approaches to use ESI-MS for fingerprinting of biodiesel sources,[19] its widespread use for non-target investigation of biodiesel aging is still underway. Since direct-injection high-resolution (HR)MS showed good results in expanding the measurable amount of compounds in crude oil samples,[20] in this study a non-target direct injection utilizing positive ion electrospray ionization in combination with ultrahigh-resolution mass spectrometry [ESI(+)-HRMS] was applied to investigate the compositional changes in two different biodiesels during long-term storage. HRMS is the method of choice for the non-target analysis of complex mixtures.[21]

Results and Discussion

Though various methods have been used to study the processes and products of biodiesel aging,[22] many of the emerging compounds have not yet been characterized in detail. Given the results of previous studies, it is expected that the biofuel components react with oxygen as a dominant transformation pathway. This uptake of oxygen can be confirmed with the results shown in the mass spectrum in Figure 1. This spectrum shows the original UCOME sample, taken before the start of the storage experiment where not only the unadulterated FAMEs but also compounds with additional oxygen are present in relatively high abundance. While such high intensities were not expected before the start of the storage period, the effect can be partly explained by the origin of the sample, made from used cooking oils, among others frying oils, which have undergone high thermal and oxidative stress before the transesterification process. In a way, a biodiesel produced from such material can be considered an already pre-aged sample. In comparison, the spectrum recorded for the RME sample before storage shows noticeable less signal intensity for oxygenated ester products (see the Supporting Information, Figure S1).

That these trace amounts of oxidized products are also found in the unaged RME sample is a positive feature of the employed analysis scheme. Electrospray is especially powerful in ionizing polar compounds, and the formation of sodium adducts is commonly favored for analytes with a high amount of oxygen in their structure. The more oxygen is incorporated into the original FAME during storage, the easier it is supposed to be ionized by ESI. This will tentatively lead to an overexpression of highly oxidized products, which on the other hand is favorable for this study, as also minute amounts of such products can be detected.

Oxygen uptake

The nature of the sample and the aforementioned reasons mean that this sample is dominated by oxygen species. From all assigned peaks, shown in the mass spectrum in Figure 1, 96.8% contained at least one oxygen atom.

During the storage of the biodiesel for 12 months in open containers, reactions with oxygen are expected. All these data are summarized in a bar chart in Figure 2, where the data of UCOME storage behavior at month 0 (Figure 2A) and month 12 (Figure 2C) is compared to the results from RME also at month 0 (Figure 2B) and month 12 (Figure 2D).

In month 0 the population (number of assigned compounds within a certain heteroatom class) was highest for the O_4 class, followed by O_2 and then O_3. During storage, the relative increase of a class population rises with the corresponding amount of oxygen atoms per molecule. The population of the O_2 class, for example, increases from 68 to 106 (+56%), while the O_5 class population rises from 42 to 180 (+328%) over the course of 12 months. For the RME sample (Figure 2D) the development is similar, however, with lower populations of oxygenated compounds from the beginning. Consequently, this leads to an even higher population increase over the time of storage.

The O_2 class starts at 38 and rises to 91 detected elemental compositions (+139%), while the O_5 class starts at 18 and climbs to 139 compositions (+672%). The emerging products from the degradation processes are thus more diverse than the starting compounds, indicating that there are various reaction pathways. Starting with the highest relative intensities in both biodiesels, the O_2 class shows the most noticeable decrease from month 0 to 12 (RME: −54%, UCOME: −64%). This illustrates the transformation of the FAMEs. On the other hand,

© 2022 The Authors. ChemSusChem published by Wiley-VCH GmbH

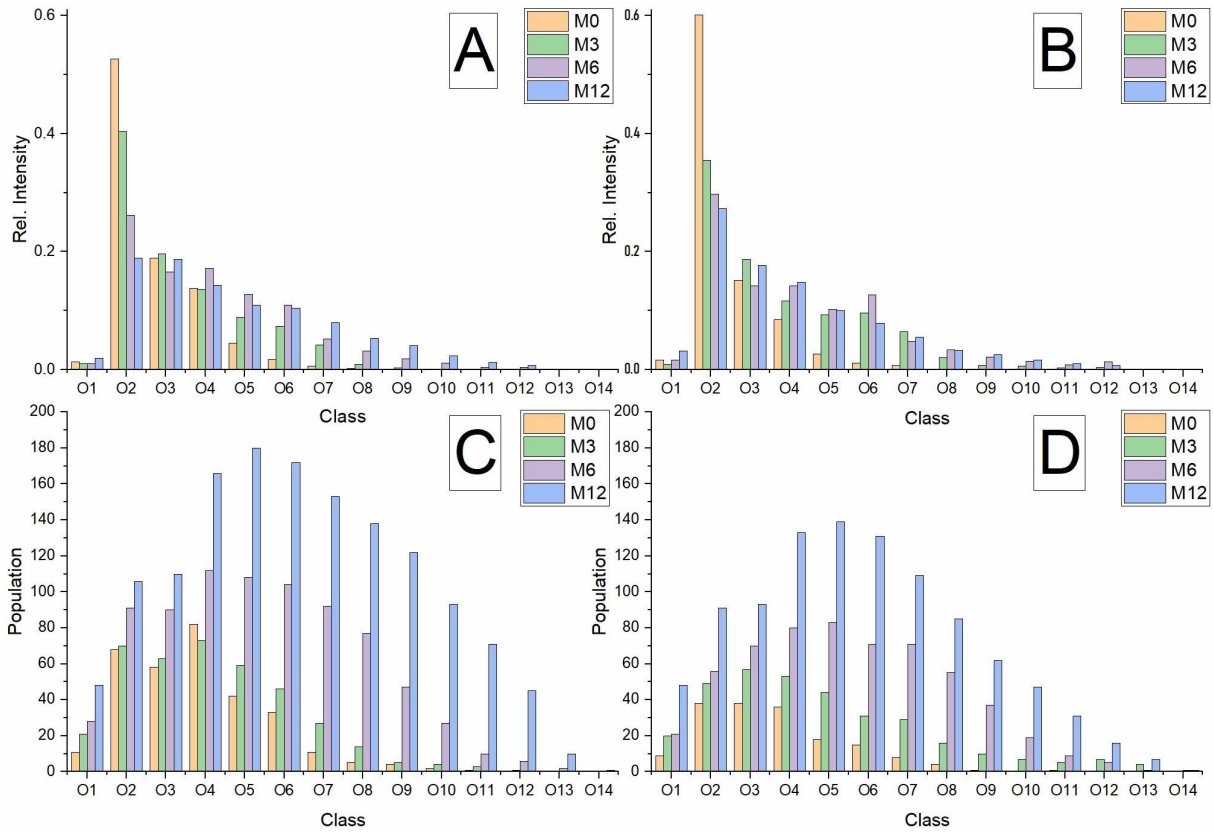

Figure 2. Population and relative intensities of (A,C) UCOME and (B,D) RME over the course of 12 months of storage.

similar to the population, the relative intensities of signals that correspond to compounds with higher amounts of oxygen per molecule increase during the storage. This indicates that the transformation is an ongoing process in which oxygen is continuously added. Also notable is the continuous amount of incorporated oxygen atoms. Mechanisms proposed so far (Frankel,[10] Schneider et al.[18]) typically include a reaction of the esters with hydro-peroxides, leading to even-numbered oxygen amounts.

Dimerization

Due to the complexity of all these reactions, there are different layers of information present in the MS data. Here, different ways of presentation need to be used. Another way of presenting the data is shown in Figure 3 (RME in Figure S2), where the results of the UCOME sample are presented in bubble plots. Compared to the bar charts in Figure 2, here those bars are further split into discrete bubbles, according to the number of carbon atoms in the corresponding molecule. Signal intensity is represented by bubble volume. The highest intensity can be seen at #C = 19 and #O = 2 (blue bubble), in which all the different unaltered FAMEs are represented. Compounds higher in *y*-direction would contain more oxygen molecules, while going into *x*-direction are compounds with higher carbon numbers. The main portion of oxidized compounds already present at the beginning of the study (M0) corresponds to oxygenated FAMEs with a carbon number of 19. These polyoxygenated FAMEs with additional oxygen uptake (more than 2 oxygen atoms per molecule) increase in intensity during the storage, hit a maximum after six months (M6), and decline afterwards. Another recognizable group of signals is observed at a carbon number of 38. These signals correspond to polyoxygenated dimeric structures of FAMEs. To differentiate such covalently bound dimers from possible Coulomb clusters, in-source fragmentation was applied, with no observable effect. It can therefore be assumed that the corresponding species are indeed covalently bound and not mere Coulomb clusters. Signals found in the area below #C = 19 can be considered as degradation products from possible C–C-bond cleavage pathways and are therefore named first degree deterioration products. Accordingly, signals found between #C = 19 and #C = 38 are most-likely the products of dimerization processes of either a FAME with a first-degree deterioration product, or two first-degree deterioration products, or the succeeding deterioration of a FAME dimer. Either way, they are products of subsequent processes and therefore considered secondary degradation products. Over the storage time, intensity shifts occur first within the group of monomeric FAMEs, with the uptake of oxygen being dominant during the first 3 months.

© 2022 The Authors. ChemSusChem published by Wiley-VCH GmbH

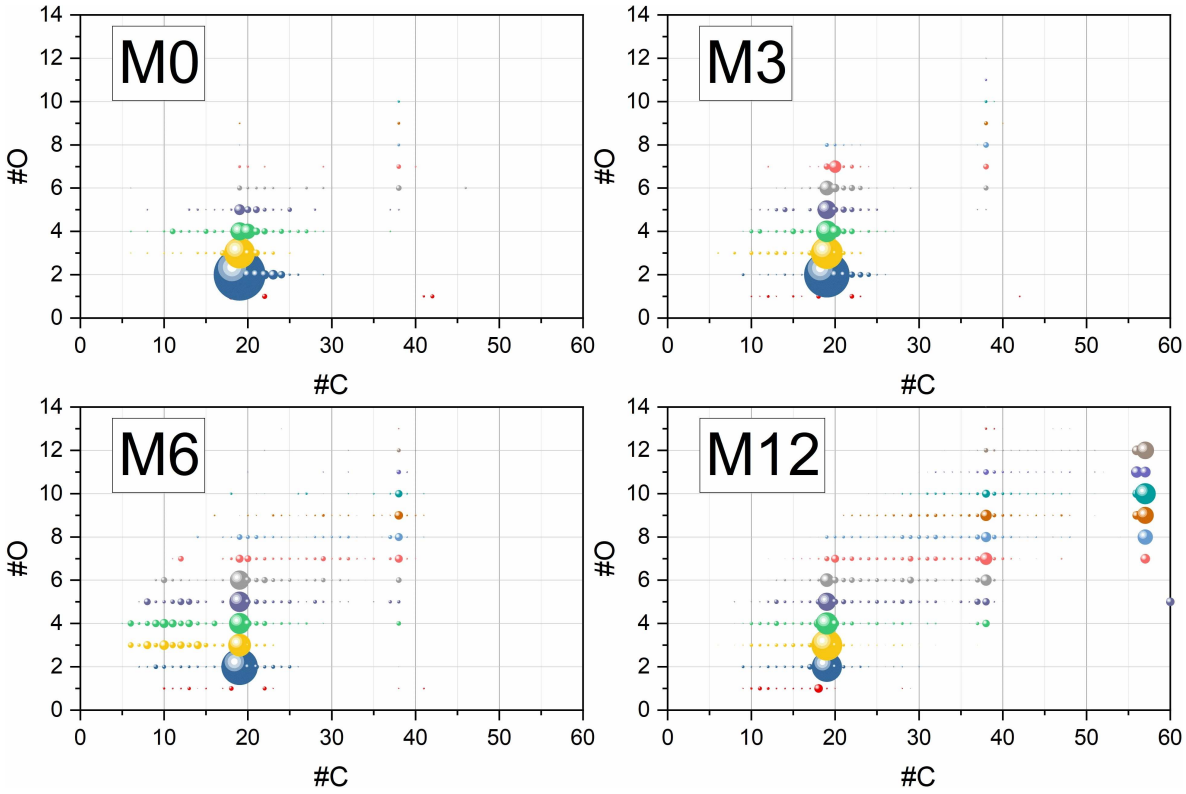

Figure 3. Bubble graph of UCOME, M0-M12. Bubble volume represents the square root of the corresponding relative intensity. The volume of the bubbles between C = 55 and C = 60 is increased by a factor of ten for better visuality. For a better visualization, the homologues series of one oxygen number (#O) is kept in the same color.

After month 6 the relative intensities of the higher-oxygenated (#O < 6) FAMEs slightly decrease.

Simultaneously, from month 6 the signals of compounds with 38 carbon atoms, which can be interpreted as dimers, are distinctively increasing in intensity. Thus, a two-step process is observed, the first step being the incorporation of additional oxygen into the FAME compounds. Only after this oxidation step a dimerization of the oxidized products is observed. These trends are also shown in Figure 4. There is a high increase in oxidized monomers during the first three months, followed by an exponential growth of the dimer intensities. This is consistent with the theoretical dimerization processes as proposed by Schneider et al.[18]

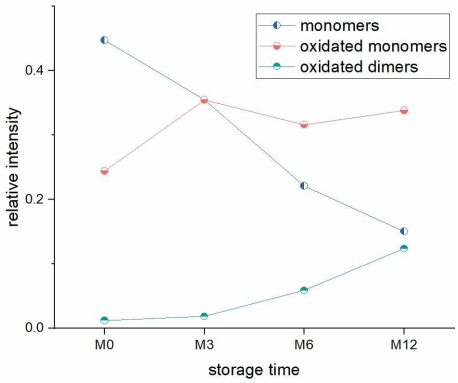

Figure 4. Development of the summed up relative intensities of the unadulterated monomers, oxidized monomers, and oxidized dimers.

The oligomerization of the fatty acid esters does not necessarily stop at dimerization. A group of signals with a carbon count of 57 in a range of #O = 7–12 occurs after 12 months of storage (Figure 3). Albeit in low intensities, these signals emerge in a pattern similar to the dimers, which, combined with their elemental composition ($C_{57}H_{94-102}O_{7-12}$) lead to the conclusion that these compounds can be interpreted as FAME-trimers. The intensities of these compounds are expected to increase further during longer storage time and open the questions how far the oligomerization would continue during storage.

In addition to UCOME, RME was also aged and studied the same way. The results are very similar, with only minor differences. The corresponding graphs can be found in the Supporting Information.

Reactivity of single esters

The determination of quantitative results from unknown compounds is difficult for detection methods without uniform response because from each compound individual calibration

© 2022 The Authors. ChemSusChem published by Wiley-VCH GmbH

curves need to be measured, which is impossible for complex mixtures. Here, methods that show a uniform response independent of the chemical nature are needed.[21a] In this case, only GC-FID is a suitable method for the determination of quantitative data, despite the difficulties mentioned in the Introduction.

In Figure 5, the results of such a study are shown. The differences in concentrations of single esters between M0 and M12 can be interpreted with different reactivity of esters. Though oleic acid methyl ester (C18:1) has the highest concentration, linoleic acid (C18:2) and linolenic acid (C18:3) methyl esters show the higher losses (-64 and −85%), corresponding to their higher reactivity due to the double bonds present in their structure.

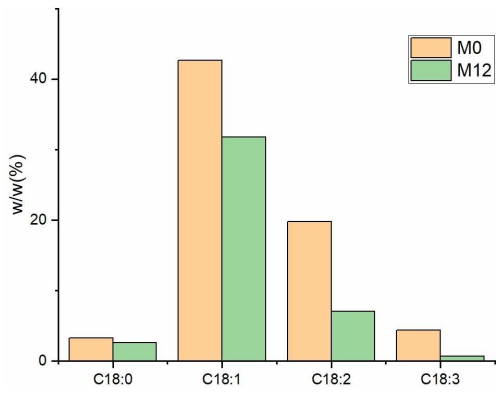

Figure 5. Concentration of the C_{18}-esters in UCOME M0 and M12. Measured by GC-FID with heptadecanoid acid methyl ester as internal standard.

This trend in reactivity is also illustrated in Figure 6. Here, the signal intensity observed for oxygenated species is shown according to the amount of hydrogen per molecule for the monomeric (C_{19}) and dimeric (C_{38}) products. Looking at the individual ester monomers, it is evident that there is a tendency for esters with less hydrogen atoms to amass higher amounts of oxygen. After twelve months of storage, compounds with 32 hydrogen atoms (e.g., C18:3) have the highest intensity in the O_8-class, which means, that six additional oxygen atoms have been incorporated. Compounds containing 34 (e.g., C18:2) or 36 (e.g., C18:1) hydrogen atoms show gradually lower intensities for higher oxygen classes. Although the bias to incorporate higher amounts of oxygen is unquestionably connected to the number of double bonds, it is not limited by it. Compounds with #H = 36 (e.g., C18:1), which contained up to five additional oxygen atoms, were measured in M12. Furthermore, oxygenated and fully saturated ester compounds with 38 hydrogen atoms were found in M0 and M12. These compounds could be formed by oxygen incorporation in fully saturated esters or by incorporation of water in esters with one double bond. Since reactivities of saturated esters are very low, the latter seems more probable.

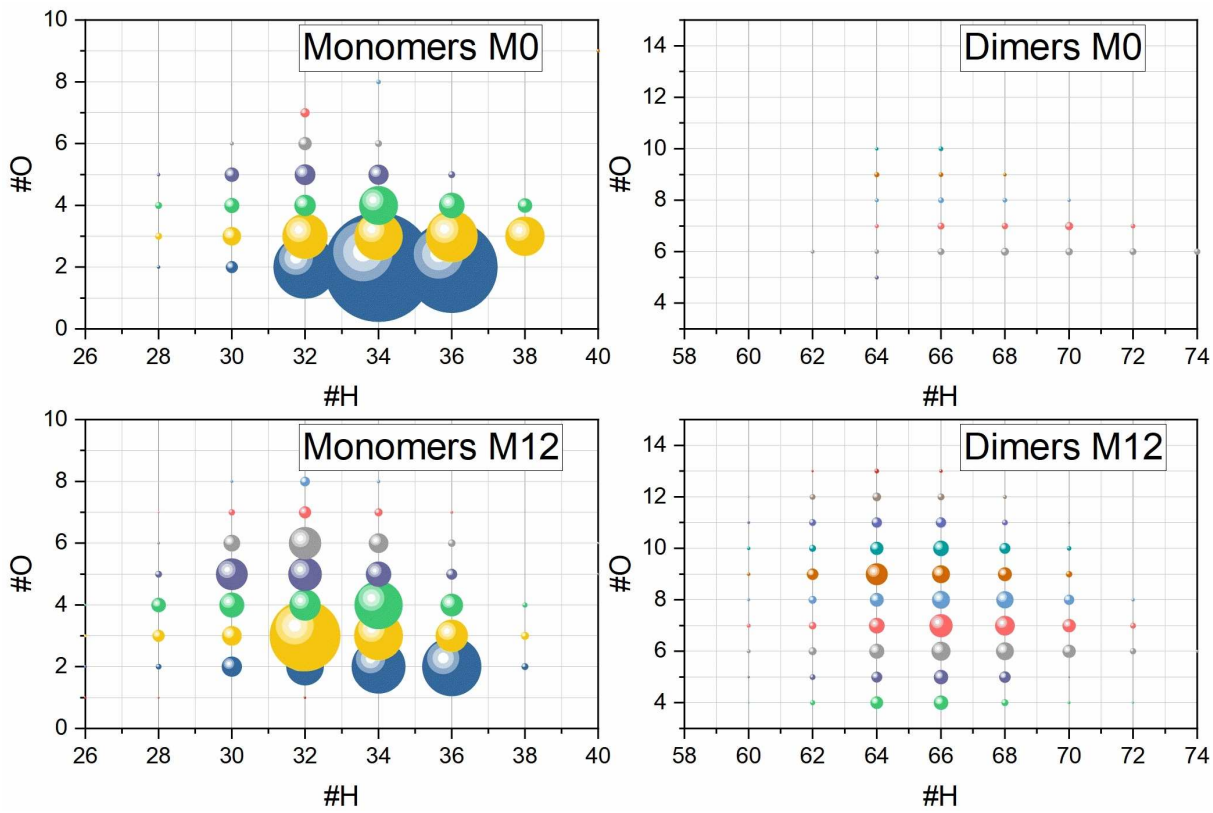

Figure 6. Bubble graphs of UCOME, M0–M12. Bubble volume represents the square root of the corresponding relative intensity. Only compounds with a carbon number of 19 (left side) or 38 (right side) were taken into account.

© 2022 The Authors. ChemSusChem published by Wiley-VCH GmbH

Another interesting finding is the high intensity for oxygenated compounds with 30 or 28 hydrogen atoms. Despite the higher polarity of oxygenated compounds, this significant increase over 12 months indicates that these compounds are produced during the degradation process. That would lead to the conclusion that there are reaction pathways where the oxygen addition is coupled with hydrogen abduction. Both findings are reiterated in the development of the dimeric esters shown in Figure 6. The overall intensity of oxygenated dimers is highest for compounds containing 64 or 66 hydrogen atoms. Both the highest intensity for a compound containing the highest oxygen number (#O = 13) and the highest intensity for low amounts of oxygen (#O = 4) are present in these two groups. Especially the high intensities for compounds with four oxygen atoms show that esters with two to three double bonds seem to have either a promoting or stabilizing effect on dimerization, even without additional oxygen.

It is worth noting that there are no dimers with more than seven additional oxygen atoms, although monomers with four or more additional oxygen atoms are available.

This indicates that dimerization is hindered by high amounts of oxygen, probably due to the inactivation of double bonds. The importance of double bonds for the dimerization is further stressed by the low intensities of dimers exclusively of oleic methyl esters (#H = 72) and the fact that dimeric structures of stearic acid methyl esters are not found, even though there are oxygenated versions of these esters present. There are also high intensities for compounds containing 62 hydrogen atoms. This again indicates a hydrogen abduction pathway for either the oxygen intake or the dimerization process.

Conclusion

Utilizing the tools of non-target screening with high-resolving Fourier-transform mass spectrometry (FTMS) methods reveals the diverse reaction products for biodiesel aging. It could be shown that oxygen incorporation is the first step for aging, followed by an accelerating dimerization and even trimerization of the FAME-molecules at the later stage of the storage period. Oxygen incorporation goes up to six additional oxygen atoms in an ester molecule and a total of seven additional oxygen atoms for an ester dimer. The higher reactivity for highly unsaturated esters also results in a greater amount of oxygen intake compared to more saturated esters. Additionally, unsaturated esters also show a greater tendency towards dimerization, even building dimers with no additional oxygen. Due to the increasing intensities of compounds containing fewer hydrogen atoms than C18:3 it is very likely that a hydrogen abstraction mechanism is one of the many aging pathways for the fatty acid methyl esters. This method bears the potential for more in-depth analysis of the oxygenated structures produced by aging, making it possible to find ways to inhibit or slow down the processes. The results shown here could indicate possible formation ways of precipitates in biodiesel/diesel blends during storage, where formation of di- and trimers could be of great significance.

Experimental Section

Sample preparation

Two different biodiesel types were used, with their physical parameters given in Table 1. They differ in their source materials. UCOME (used cooking oil methyl esters) are made from recycled cooking oils (e.g., frying oils), while RME (rapeseed methyl esters) is produced from fresh rapeseed oil. The biodiesel samples were then aged in open glass bottles in a heated storage closet at 40 °C for up to twelve months. Samples were stored in twelve aliquots for monthly probing. After sampling, an aliquot of 100 ppm in methanol (J.T. Baker, ultra HPLC grade) was obtained, and the remainder of the samples were stored at −20 °C.

Instruments and methods

All mass spectra were collected on a research-type Orbitrap Elite MS (Thermo Scientific, Bremen, Germany), using an electrospray ionization source in positive mode [ESI(+)] at 4 kV ionization voltage. Mass spectra were recorded over a range of $150 \leq m/z \leq 1000$ with a resolution setting of $R = 480000$ (full width at half-maximum at $m/z = 400$). Spectral stitching was used with scan windows of 30 Da and a 5 Da overlap.[20,23]

GC-FID measurements were conducted on an Agilent 7890B with a DB-Wax-Ether column (Agilent) ($L = 30$ m, I.D. = 0.25 mm). The carrier gas was H_2 at 0.6 bar, and the temperature was increased from 35 to 280 °C at 5 °C min^{-1} and held at 280 °C for 5 min. The injector had a temperature of 220 °C, the analyzer one of 350 °C.

Data

Elemental composition assignment and internal recalibration of recorded spectra were performed using Composer (Version 1.5.3, Sierra Analytics, Modesto, CA, USA, with a maximum mass accuracy error better than 1 ppm. Compositional constraints were set to allow proton or sodium ion adducts of compositions in the range of $C_{0\text{-}200}H_{0\text{-}1000}O_{0\text{-}20}N_{0\text{-}3}$ with a double bond equivalent (DBE) of −0.5 to 40.

Acknowledgements

Generous financial funding from the Bundesministerium für Wirtschaft und Energie through the IGF Project (IGF 19965N by DGMK 791) is gratefully acknowledged. The authors thank Dr. David Stranz (Sierra Analytics, Modesto, CA, USA) for access to new data handling software. The authors also thank Simon Eiden, Nina Mebus and Sebastian Feldhoff (Öl-Wärme-Institut (OWI) Aachen, Germany) for providing aged biofuel samples for this study. Open Access funding enabled and organized by Projekt DEAL.

Table 1. Properties of the two biodiesel types used in this project.

Biodiesel	Water content [mg kg^{-1}]	Ester content [%*w*/*w*] C16:0	C18:0	C18:1	C18:2	C18:3
UCOME	148	10.6	3.5	47.2	20.6	4.6
RME	264	4.1	1.8	56.2	19.7	10.0

© 2022 The Authors. ChemSusChem published by Wiley-VCH GmbH

Conflict of Interest

The authors declare no conflict of interest.

Data Availability Statement

Research data are not shared.

Keywords: aging · biodiesel · electrospray ionization · lipid oxidation · mass spectrometry

[1] H. Andruleit, M. Blumenberg, J. Kus, J. Meßner, M. Pein, D. Rebscher, M. Schamel, M. Schauer, M. Schmidt, S. Schmidt, G. von Goerne, *BGR Energiestudie 2017 – Daten und Entwicklungen der deutschen und globalen Energiversorgung* **2017**, *21*.
[2] a) P. H. Carr, *Nat. Sci.* **2013**, *5*, 130–134; b) B. Islam, *Int. J. Chem. Sci.* **2013**, *11*, 1426–1436.
[3] *Gesetz zum Schutz vor schädlichen Umwelteinwirkungen durch Luftverunreinigungen, Geräusche, Erschütterungen und ähnliche Vorgänge (Bundes-Immissionsschutzgesetz-BImSchG)*, **2021**.
[4] G. Knothe, J. Krahl, J. Van Gerpen, *The biodiesel handbook*, 2 ed., AOCS Press, USA, **2015**.
[5] *Evaluations- und Erfahrungsbericht für das Jahr 2018*, **2019**.
[6] R. E. Teixeira, *Green Chem.* **2012**, *14*, 419–427.
[7] E. Carota, M. Petruccioli, A. D'Annibale, A. M. Gallo, S. Crognale, *Appl. Microbiol. Biotechnol.* **2020**, *104*, 4617–4628.
[8] R. A. Lee, J.-M. Lavoie, *Anim. Front.* **2013**, *3*, 6–11.
[9] J. Orsavova, L. Misurcova, J. V. Ambrozova, R. Vicha, J. Mlcek, *Int. J. Mol. Sci.* **2015**, *16*, 12871–12890.
[10] E. N. Frankel, *Lipid oxidation, Vol. 18*, 2 ed., The Oily Press, England, **2014**.
[11] J. P. Szybist, J. Song, M. Alam, A. L. Boehman, *Fuel Process. Technol.* **2007**, *88*, 679–691.
[12] G. Knothe, K. R. Steidley, *Energy Fuels* **2005**, *19*, 1192–1200.
[13] a) F. Bär, H. Hopf, M. Knorr, J. Krahl, *Fuel* **2018**, *232*, 108–113; b) K. Bacha, A. Ben-Amara, A. Vannier, M. Alves-Fortunato, M. Nardin, *Energy Fuels* **2015**, *29*, 4345–4355; c) L. Botella, F. Bimbela, L. Martín, J. Arauzo, J. L. Sánchez, *Front. Chem.* **2014**, *2*; d) M. Murta Valle, R. Leonardo, J. Dweck, *J. Therm. Anal. Calorim.* **2014**, *116*, 113–118; e) J. Pullen, K. Saeed, *Renewable Sustainable Energy Rev.* **2012**, *16*, 5924–5950.
[14] A. Haseeb, H. H. Masjuki, L. Ann, M. Fazal, *Fuel Process. Technol.* **2010**, *91*, 329–334.
[15] a) C. Bannister, C. Chuck, M. Bounds, J. Hawley, *Proc. Inst. Mech. Eng. Part D* **2011**, *225*, 99–114; b) K. Gopalan, C. J. Chuck, C. Roy-Smith, C. D. Bannister, *SAE Int. J. Adv. Curr. Pract. Mob.* **2019**, *1*, 284–290.
[16] S. Flitsch, P. M. Neu, S. Schober, N. Kienzl, J. r. Ullmann, M. Mittelbach, *Energy Fuels* **2014**, *28*, 5849–5856.
[17] a) S. Marmesat, J. Velasco, M. Dobarganes, *J. Chromatogr. A* **2008**, *1211*, 129–134; b) O. Berdeaux, S. Fontagné, E. Sémon, J. Velasco, J. L. Sébédio, C. Dobarganes, *Chem. Phys. Lipids* **2012**, *165*, 338–347.
[18] C. Schneider, N. A. Porter, A. R. Brash, *J. Biol. Chem.* **2008**, *283*, 15539–15543.
[19] a) I. Eide, K. Zahlsen, *Energy Fuels* **2007**, *21*, 3702–3708; b) R. R. Catharino, H. M. Milagre, S. A. Saraiva, C. M. Garcia, U. Schuchardt, M. N. Eberlin, R. Augusti, R. C. Pereira, M. J. Guimarães, G. F. de Sá, *Energy Fuels* **2007**, *21*, 3698–3701.
[20] A. Vetere, W. Schrader, *ChemistrySelect* **2017**, *2*, 849–853.
[21] a) A. Vetere, D. Pröfrock, W. Schrader, *Angew. Chem. Int. Ed.* **2017**, *56*, 10933–10937; b) Y. Xu, W. Schrader, *Energies* **2021**, *14*, 2032; c) R. Luo, W. Schrader, *J. Hazard. Mater.* **2021**, *418*, 126352; d) P. Benigni, K. Sandoval, C. J. Thompson, M. E. Ridgeway, M. A. Park, P. Gardinali, F. Fernandez-Lima, *Environ. Sci. Technol.* **2017**, *51*, 5978–5988; e) J. V. Headley, K. M. Peru, S. Mishra, V. Meda, A. K. Dalai, D. W. McMartin, M. M. Mapolelo, R. P. Rodgers, A. G. Marshall, *Rapid Commun. Mass Spectrom.* **2010**, *24*, 3121–3126; f) J. V. Headley, K. M. Peru, M. P. Barrow, *Mass Spectrom. Rev.* **2016**, *35*, 311–328; g) K. Qian, R. P. Rodgers, C. L. Hendrickson, M. R. Emmett, A. G. Marshall, *Energy Fuels* **2001**, *15*, 492–498; h) E. Smit, C. P. Rüger, M. Sklorz, S. De Goede, R. Zimmermann, E. R. Rohwer, *Energy Fuels* **2015**, *29*, 5554–5562; i) C. P. Rüger, M. Sklorz, T. Schwemer, R. Zimmermann, *Anal. Bioanal. Chem.* **2015**, *407*, 5923–5937; j) J. F. Zhang, Y. Jiang, L. F. Easterling, A. Anstner, W. R. Li, K. Z. Alzarieni, X. M. Dong, J. Bozell, H. I. Kenttamaa, *Green Chem.* **2021**, *23*, 983–1000.
[22] C. J. Chuck, C. D. Bannister, R. W. Jenkins, J. P. Lowe, M. G. Davidson, *Fuel* **2012**, *96*, 426–433.
[23] A. Gaspar, W. Schrader, *Rapid Commun. Mass Spectrom.* **2012**, *26*, 1047–1052.

Manuscript received: March 2, 2022
Revised manuscript received: April 8, 2022
Accepted manuscript online: May 5, 2022
Version of record online: May 30, 2022

© 2022 The Authors. ChemSusChem published by Wiley-VCH GmbH